J Mater Sci (2010) 45:1179–1188
DOI 10.1007/s10853-009-4062-y

Ultra-long SiO_2 and SiO_2/TiO_2 tubes embedded with Pt nanoparticles using magnus green salt as templating structures

Catherine Aresipathi · Armin Feldhoff · Michael Wark

Received: 23 August 2009 / Accepted: 21 November 2009 / Published online: 4 December 2009

Abstract For the first time, magnus green salt (MGS, $[Pt(NH_3)_4][PtCl_4]$) fibers precipitated by solvent modification have been employed as a structure-directing modifier to synthesize single silica and silica/titania microtubes via a sol–gel process. In the case of titania tubes, tetraethylorthosilicate must be used as a capping agent to hinder the aggregation of primary MGS fibers and to serve as a protective layer against thermal stress during the metal salt fiber reduction. This implies that SiO_2/TiO_2 tubes result. The synthesized tubular materials were imaged by scanning and transmission electron microscopy, while their composition was determined by energy dispersive X-ray analysis and thermogravimetric analysis. Crystallinity and thermal stability of the tube walls were studied using X-ray diffraction analysis. The obtained oxide tubes possess high aspect ratios (80–200) because they are up to 60 μm in length, but only 300–700 nm in thickness. The key aspects of the synthesis approach are that the templating MGS fibers control the internal diameter of the oxide tubes, while the synthesis conditions control their wall thickness. The suggested method is a simple approach which produces, at low temperatures, very long oxide tubes with a very high amount of Pt (48–51 wt%) directly incorporated inside the tubes. To the best of our knowledge, filling of SiO_2 or SiO_2/TiO_2 nanotubes with such a dense population of Pt metal nanoparticles has not been demonstrated so far; our own experiments with $[Pt(NH_3)_4](HCO_3)_2$ as templating salt formed only tubes containing about 40 wt% Pt and were only about 20 μm long. The now formed more Pt-rich tubes are expected to have vivid applications in (photo) catalysis and in fabricating novel devices, such as nano- or sub-microcables.

C. Aresipathi · A. Feldhoff · M. Wark (✉)
Institute of Physical Chemistry and Electrochemistry, Leibniz University of Hannover, Callin Str. 3a, 30167 Hannover, Germany
e-mail: michael.wark@pci.uni-hannover.de

Introduction

Inorganic oxide nanostructures, e.g., nanoribbons [1], nanorods [2], and nanotubes (NTs) [3], are under constant investigation owing to their potential for emerging applications in solar energy devices [4–6], gas sensors [7], drug delivery systems [8], hydrogen fuel storage [9], single-DNA sensing [10], pollutants decomposition [11], or for nanoscale electronic and optical devices such as transistors or light emitting diodes [12]. The applications utilize the inherent characteristics of the tubular oxide nanostructures that possess large surface areas, narrow inner pores, and surface catalytic properties.

In recent years, diverse inorganic tubes consisting of metals [13], boron or metal nitrides [14], metal sulfides [15], and metal oxides [16] were reported. Especially, nano- or microtubes of TiO_2 attracted tremendous attention because of their strong oxidizing capability, chemical inertness, and nontoxicity, rendering them prospective for use in heterogeneous catalysis [17], electrocatalysis [18], photocatalysis [19] including photocleavage of water [20], dye-sensitized solar cells [21], and corrosive protective or optical coatings [22]. Recently, synthesis and application aspects have been summarized in two review papers [23, 24].

Nakahira et al. [25] and Adachi et al. [26] reported that TiO_2 NTs by themselves do not exhibit high photocatalytic properties although they show high light absorption as well as from their high surface area high adsorption ability. Akita et al. [27] proved that TiO_2 NTs need noble metal encapsulation to show improved photocatalytic properties.

Others claimed that the introduction of catalytic metals such as Au, Pt, Pd, and Nb into metal oxides not only amend the sensing performances but also their crystalline structure [28]. This was evident from the research group of Epifani et al. [29] who observed that Pt-incorporated TiO_2 nanostructures displayed enhanced sensitivity to H_2 when compared to its pure counterpart. Sato et al. [30] found that the catalytic activity and selectivity for methanol in CO-H_2 reaction was extraordinarily high when Pt-embedded TiO_2 NTs were used as catalysts. Hence, a simplified synthesis approach to prepare metal-doped titania containing NTs becomes a challenging task.

Traditionally, metals can be incorporated into presynthesized SiO_2 NTs by subsequent methods like chemical vapor deposition, evaporation by arc discharge, or physically by employing capillary forces [31]. However, most often, the degree of loading by these routes is restricted to low weight percentage [32].

Although template-directed synthesis of NTs limits their dimensions to those of the template, it stands advantageous over the conventional hydrothermal synthesis because of its facile fabrication, diversity in composition of materials, and uniform size distribution of the obtained NTs [33]. Numerous templates were explored to synthesize oxide NTs such as metal nanorods [34], anodized aluminum oxide (AAO) membranes [35], or electrospun poly(L-lactide) fibers [36].

Our group was the first to synthesize SiO_2 and TiO_2 tubes availing metal salt fibers as templating structures [37, 38]. This method is advantageous as the formation of tubes and their filling is combined in a single step. Strictly spoken, the obtained tubes are not NTs because their lengths as well as their diameters mostly exceed 100 nm, but the diameters stay in the sub-micrometer regime. Thus, henceforth we will call them microtubes or simply tubes. By using uniformly grown and well-dispersed $[Pt(NH_3)_4](HCO_3)_2$ fibers as structure-directing agents in a sol–gel-derived coating process, SiO_2 tubes with as much as 40 wt% Pt incorporated inside could be synthesized [39]. The use of a comparable Co salt ($[Co(NH_3)_6](HCO_3)(CO_3)$) led to silica tubes with Co nanoparticles inside the tube interior, aligned to chains due to the magnetic dipolar interactions between neighboring particles [40]. The samples show a characteristic feature of ferromagnetism with a magnetically anisotropic barrier attributed to the shape anisotropy of the one-dimensional arrangement of Co-based nanoparticles within the SiO_2 tubes [41].

In this study, we report the synthesis of ultra-long SiO_2 and SiO_2/TiO_2 tubes doped with explicitly higher amount of Pt using fibers of tetramineplatinum tetrachloroplatinate $[Pt(NH_3)_4][PtCl_4]$, popularly called magnus green salt (MGS), as templating structures. We were able to synthesize SiO_2 tubes effectively with lengths up to 60 μm and diameters in the range of 300–700 nm hosting 48–51 wt% of Pt nanoparticles in their interior voids. To the best of our knowledge, synthesis of oxide microtubes with such high aspect ratio (200) and such high content of guest species has not been demonstrated so far, and Pt-incorporated SiO_2/TiO_2 tubes could be obtained in a single step as well. Moreover, this facile approach could not only reduce synthesis time but is also cost effective.

Experimental details

Chemicals

Reagents used in the synthesis of Pt-embedded SiO_2 and SiO_2/TiO_2 tubes include tetraamineplatinum tetrachloroplatinate (MGS, 97%, Aldrich), titanium isopropoxide (TIP, 97%, Aldrich), tetramethylammonium hydroxide (TMAOH, 25%, Aldrich), tetraethylorthosilicate (TEOS, 98%, Aldrich), isopropanol (99.9%, Merck), and deionized H_2O. All the commercial extra pure reagents were used as received.

Synthesis of ultra-long SiO_2 tubes with encapsulated Pt metal

First, MGS fibers have to be precipitated. For this purpose, typically, 0.0042 mmol of MGS is dispersed in 2 mL of aqueous ammonia solution (0.4 N). To this solution, 2 mL of ethanol is added at a stirring rate of 300 rpm. Subsequently, the mixture is placed in an ice bath (0 °C) for 10 min.

To couple the rate of hydrolysis of TEOS and its interaction with the template fibers, various parameters such as aging time, amount of TEOS and water, temperature, and pH of the solution were varied. The optimized recipe to synthesize SiO_2 tubes using MGS as template is given below.

14 μL of TEOS is added dropwise into the MGS fiber stock solution and stirred for 2 min. After increasing the rate of stirring to 1000 rpm, 0.1 mL of ethanol is injected swiftly. After a few minutes, the stirring rate can be again reduced to 300 rpm, and 10 mL of ethanol is added slowly at a rate of 0.5 mL/min. The reaction is aged in the cold bath for 3 h and then allowed to warm up to room temperature within 4 h. The obtained product is washed with water and dried at room temperature. The dried samples were calcined at 280 °C for 6 h with a heating rate of 1 °C/min.

Synthesis procedure of SiO_2/TiO_2 tubes with encapsulated Pt metal

The synthesis of $Pt/SiO_2/TiO_2$ tubes is carried out in two steps: (a) stabilization of TIP and (b) formation of the tubes.

Stabilization of TIP

The stabilization process of TIP with TMAOH in the presence of water at room temperature was carried out according to a method described by Ohya et al. [42]. However, the concentrations of the reagents have been slightly altered. 0.05 M TIP is dropped into 0.1 M TMAOH solution resulting in the formation of an opaque colloidal solution. Under continuous stirring at 300 rpm, the transparency of the solution increases slowly and stirring is maintained until it is fully transparent. Typically, a clear solution was observed after 96–120 h.

Formation of Pt/SiO_2/TiO_2 tubes

The synthesis of the TiO_2 containing tubes requires lower temperature than for SiO_2 tubes. Thus, in this case, the MGS stock solution is cooled down to −25 °C in a cold bath of ethanol and liquid nitrogen. To the cooled solution, 14 μL of TEOS is added under rapid stirring (>1000 rpm). Shortly after this (at most 2 min later), the stabilized TIP solution is added dropwise. After 2 min, 0.1 mL of isopropanol is injected swiftly. After a few minutes, the stirring rate is reduced to 300 rpm and 10 mL of isopropanol is added within 20 min. The reaction mixture is aged in the cold bath for 3 h and then allowed to warm up to room temperature within 4 h.

Again, the oxide tubes obtained are washed with water, dried at room temperature, and calcined in air at 280 °C for 6 h with a heating rate of 1 °C/min.

Characterization

The dimensions of the tubes and their morphologies were analyzed by field-emission scanning electron microscope (FE-SEM, JEOL JSM-6700F) with low excitation voltages in the range of 0.5–2 kV. Ethanolic suspensions of the samples were directly dropped onto a polished surface of a brass sample holder and analyzed after the solvent evaporation. The inner structures of the tubes were observed by (scanning) transmission electron microscopy ((S)TEM) employing bright-field and high-angle annular dark-field contrast. A JEOL JEM-2100F electron microscope with a UHR pole piece providing a point resolution better than 0.19 nm was used at 200 kV. Additionally, the microscope is equipped with an Oxford Instruments INCA-200-TEM system with an ultra-thin window that allows elemental analysis by energy-dispersive X-ray spectroscopy (EDXS). To obtain specimen for TEM, the calcined powder was put onto a 300-mesh copper-supported carbon foil (Quantifoil).

The crystal phases of the Pt/SiO_2/TiO_2 tubes were evaluated by X-ray diffraction (XRD) patterns recorded on a Philips X'Pert-MPD instrument using monochromatic Cu-Kα radiation at 40 kV, a slit width of 0.15 mm, and a count rate of 5 s per step. Thermogravimetric (TGA) measurements were carried out on a Netzsch STA429 thermoanalyzer from room temperature to 1000 °C at a heating rate of 1 °C/min in air.

Results and discussion

Formation of polydisperse fibers from MGS

MGS is a quasi one-dimensional compound comprising chains of alternating $[Pt(NH_3)_4]^{2+}$ and $[PtCl_4]^{2-}$ moieties giving linear arrays of platinum atoms separated by a distance of 0.325 nm as illustrated in Fig. 1 [43]. This inter-platinum distance is larger than the typical bond length of 0.26–0.28 nm found, e.g., in metallic Pt [44]. Hence, the linear arrangement of the platinum atoms is mainly determined by the electrostatic interactions between the oppositely charged coordination units rather than by bonds between the platinum atoms, although the Pt–Pt interactions still exist [45].

SiO_2 and SiO_2/TiO_2 tubes with platinum particles encapsulated are synthesized as shown schematically in Fig. 2. In the first instance, template fibers of MGS are prepared by the re-precipitation of salt from an aqueous solution by the addition of ethanol. The solubility of MGS is lower in ethanol solution compared to water as solvent. Later, the fibers are coated with a metal alkoxide (TEOS and TIP) in a sol–gel process. Subsequently, calcination at 280 °C destroys the ionic complexes and reduces the Pt ions into metal Pt, which either diffuse into the porous walls of SiO_2 or reside inside the tubes based on the conditions applied.

Figure 3a depicts the SEM micrograph of commercially bought pristine MGS, which already exhibits one-

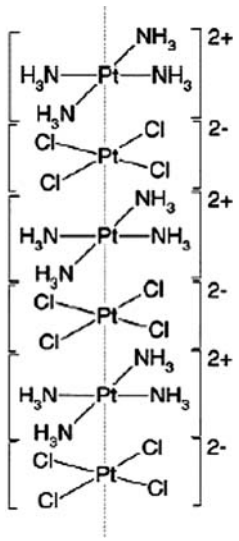

Fig. 1 Schematic illustration of the crystal structure of magnus green salt (MGS)

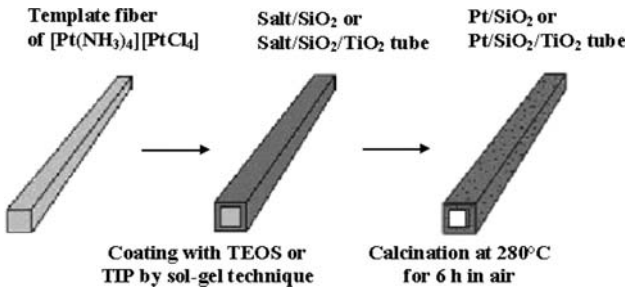

Fig. 2 Schematic representation of synthesis process of Pt containing SiO_2 or SiO_2/TiO_2 tubes using fibers of the MGS $[Pt(NH_3)_4][PtCl_4]$ as template

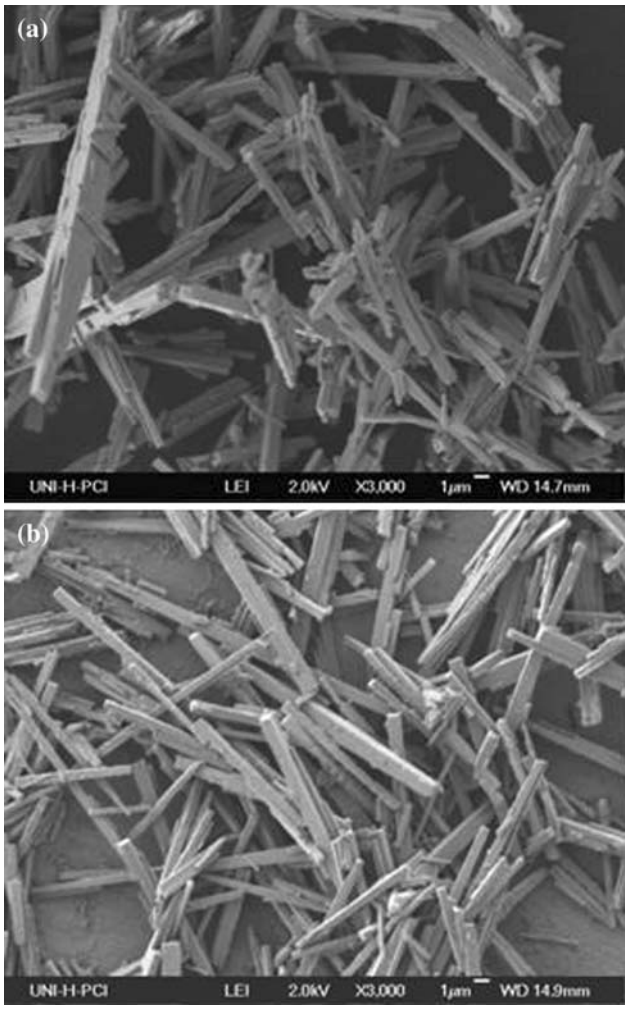

Fig. 3 SEM images of commercial MGS (**a**) and MGS fibers obtained by reprecipitation with ethanol (**b**)

dimensional morphology. Although the structures are not regular, they manifest unambiguously rectangular edges. The size distribution of the MGS structures, however, is rather broad. While some of the fibrous structures are less than 5 μm in length, most of them exhibit lengths of 10–30 μm and a few reach around 100 μm. These MGS structures when dispersed in ammonia solution were not dissolved completely. To have uniform formation of nanostructures, the nondissolved fraction of salt was separated. Subsequent reprecipitation of the dissolved fibrous structures by the addition of the same volume of ethanol yielded much more uniform MGS fibers typically 20–30 μm long and quite regularly in diameter (300–700 nm) as shown in Fig. 3b. The regular geometry displayed by the Pt template fibers indicate its internal periodicity. During the reprecipitation process, the dropwise addition of ethanol leads the MGS in the aqueous solution to concentrate forming building blocks. These aggregates form nuclei through homogenous nucleation and grow anisotropically due to differences in the surface energies of their different faces. A similar anisotropic growth was also observed for $[Pt(NH_3)_4](HCO_3)_2$ fibers [39].

Synthesis of high aspect ratio MGS/SiO_2 fibers

Scanning electron micrographs shown in Fig. 4 from as-synthesized MGS/SiO_2 tubes prove the regularity of the fibrous structures. The majority of fibers exhibited diameters in the range of 300–700 nm. Since the fibers are up to 60 μm long, aspect ratios of about 80–200 result. The length of the silica tubes is on average increased with respect to the templating fibers demonstrating that the coating with SiO_2 is by itself anisotropic.

When added to the stock solution TEOS undergoes intensive hydrolysis. To promote the hydrolysis of TEOS aqueous, NH_3 acts as a base catalyst, wherein the silicate monomers deprotonate and adsorb on the specific facets of the fibrous MGS nuclei in the stock solution. The resulting negatively charged silicate monomers might behave as electron donors and form hydrogen bonds with the ammine ligands of the cationic Pt^{2+} complex in the MGS. However, the interaction occurs with different probabilities on the different facets of the salt fibers. In the growth direction of MGS less $[Pt(NH_3)_4]^{2+}$ units are available than on the side facets of the fibers and thus the coating with silicate monomers is hampered. Moreover, the small faces at the top and bottom side of the MGS fibers are attractive for an interaction with other fibers because top-end $[Pt(NH_3)_4]^{2+}$ units can interact with bottom-end $[PtCl_4^{2-}]$ units. This attractive interaction promotes the formation of MGS/SiO_2 fibrous structures even longer than the original MGS fibers. Owing to these interactions with the template, a layer of silanol molecules adsorbs on the surface of the template and subsequently the follow-up adsorbates (TEOS monomers) deposit on the first layer and more –Si–O–Si– bonds are formed by rapid condensation leading to thicker walls. In addition, maintaining the reaction temperature to 0 °C is important as it slows down the hydrolysis and condensation rate to values sufficiently low that the soluble silicates are

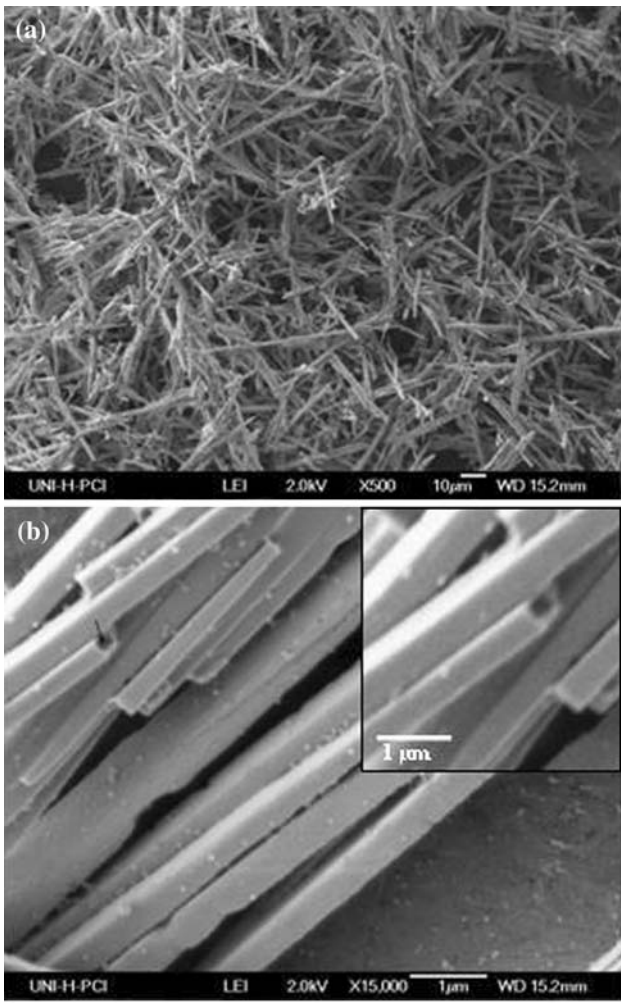

Fig. 4 SEM micrographs revealing high aspect ratios (80–200) (**a**) and narrow size distribution of Pt-filled SiO_2 tubes (**b**)

only polymerized on the surface of the template and any unwanted formed morphologies are thwarted from aggregating.

General aspects in the synthesis procedure of tubular TiO_2 structures

The chemical modification of titanium alkoxides with stabilizers is a well-known procedure in the sol–gel processing to stabilize the alkoxide molecules against uncontrolled hydrolysis upon water addition. Mostly β-diketones, and in particular acetylacetone, are used to stabilize metal alkoxides toward hydrolysis reactions [46]. Jiang et al. [47] observed that glycolate-stabilized precursors are resistant against precipitation even when left exposed to air for several days. In this study, the alkoxide precursor was coupled with TMAOH which resulted in a colorless clear solution without any formation of dense colloidal species. Results of Ohya et al. [42] suggest that titanic acid, H_2TiO_3, derived from the hydrolysis of TIP undergoes an acid–base reaction with amines to yield alkyl ammonium titanates $[R_4N]_2[TiO_3]$. The reaction schemes are proposed as following.

Hydrolysis reaction:

$$\mathrm{Ti(OCHR_2)_4 + 3H_2O \rightarrow H_2TiO_3 + 4CHR_2OH} \quad (1)$$

Acid−base reaction:

$$\mathrm{H_2TiO_3 + 2R_4NOH \rightarrow [R_4N]_2[TiO_3] + 2H_2O} \quad (2)$$

with R: $-CH_3$

The formation of clear aqueous titanate solution was found to be merely dependent on the basicity of the solution. With a strong base like TMAOH (pH >12), neutral alkyl ammonium titanates result, while in weaker basic solutions, amorphous precipitates form.

Another key aspect in the synthesis is the employment of a capping agent. In our earlier work, TEOS was utilized as a capping agent, which effectively stabilized the primary $[Pt(NH_3)_4](HCO_3)_2$ fibers from aggregation leading to the controlled growth of Pt containing silica tubes [39]. Similarly, Sun and Xia [48] achieved high aspect ratios (approx. 1000) of silver nanowires in the presence of poly vinyl pyrrolidone (PVP) which adsorbed on the surfaces of silver nanoparticles and hindered them from aggregation. In this study, we observed that TEOS not only acts as a capping agent but also served as a protective layer for the MGS fibers avoiding thermal stresses.

Structural characterization of SiO_2/TiO_2 tubes

Figure 5 illustrates SEM images of formed SiO_2/TiO_2 tubes, which morphology is determined by the crystal shapes of the template complexes as shown in Fig. 1. From the SEM images (Fig. 5a, b), it can be noticed that the tubular structures exhibit lengths in the broad range of 4–15 μm. Figure 5c shows that the tubes possess rectangular cross-section with the tube ends being mostly closed. To study the thickness of the tube walls, the as-synthesized $MGS/SiO_2/TiO_2$ tubes were slightly crushed in a mortar and observed by scanning electron microscopy which showed that the tubes had a wall thickness of about 80 nm (Fig. 5d). The tubes were distinctly thicker than those of the pure MGS/SiO_2. With TIP, the coating proceeds less uniform than with TEOS, i.e., less regular walls result and higher wall thickness is necessary to obtain crack-free walls. The condensation of TIP on the first hydrolyzed silica precursor layer (from TEOS) forms Ti–O–Si bonds according to Eq. 3.

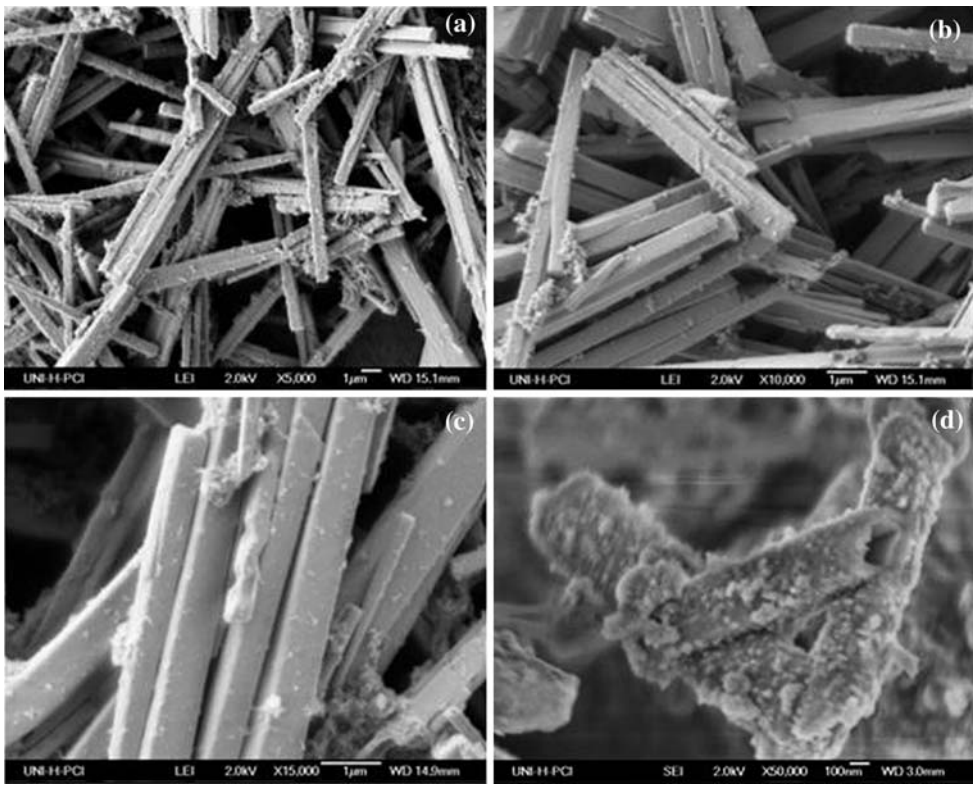

Fig. 5 SEM images of Pt-filled SiO_2/TiO_2 tubes showing uniform tubes with diameter in the range of 300–700 nm at lower (**a**) and higher magnification (**b**), respectively. **c** High magnification image depicting closed ends of tubes. **d** Image depicting the thickness of the tubes (80 nm) at higher magnification

$$\equiv Ti\text{–}OR + HO\text{–}Si\equiv \longrightarrow \equiv Ti\text{–}O\text{–}Si\equiv + ROH \quad (3)$$

Delattre and Babonneau [49] observed that the different rates of hydrolysis of silicon and titanium alkoxides can cause phase separation during sol–gel process. Hence, TIP was modified by the chelating agent TMAOH, which reduces the reactivity. Pickup et al. [50] noticed that such stabilized titanates form stronger Ti–O–Si bonds compared to samples without modification. In our study, samples prepared without stabilizing TIP displayed no traces of titanium in the tubes, while the one with stabilized TIP showed significant titanium peaks in the EDX spectra, thus supporting the higher strength of Ti–O–Si bonds (Fig. 6). Moreover, the addition of TEOS into the mixture enhanced the strength of the MGS fibers in the gel and helped in increasing resistance to the thermal stress. In the absence of TEOS, only strongly deformed TiO_2 tubes were found after drying at 80 °C. A similar observation was made by Rajesh Kumar et al. [51] who reported that addition of Si to TIP reduced drying stress as well as improved the surface area. They also realized that the use of solvents of low polarity, like the isopropanol in our case, leads to weaker hydrogen bonds, with surface hydroxyl groups reducing the strain and affecting the gel structure less strongly during drying.

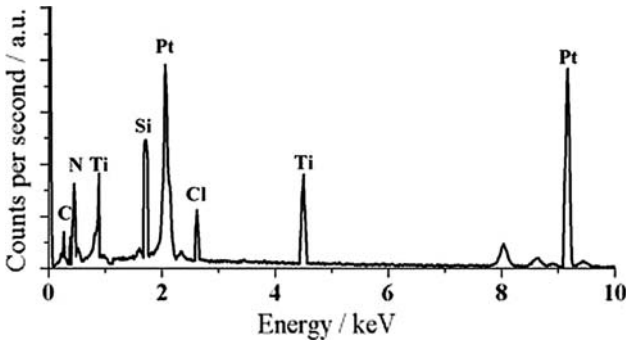

Fig. 6 EDX spectrum of $MGS/SiO_2/TiO_2$ tubes after calcination at 280 °C

Further inspection on the EDX analysis from Fig. 6 ensures the presence of elements such as platinum, nitrogen, and chlorine obtained from the MGS template apart from Ti and Si.

Formation of Pt nanoparticles in the SiO_2 tubes

Upon calcination at 280 °C, for 6 h in air, the structure-directing MGS fibers were reduced to Pt. This is elucidated in Fig. 7 from the TGA curves. During the calcination process, the Pt salt decomposes according to autoreduction (Eq. 4).

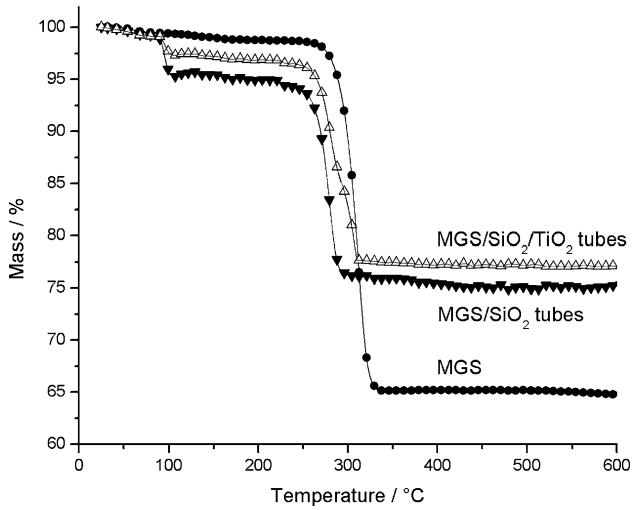

Fig. 7 Thermogravimetric curves of MGS fibers, MGS/SiO_2, and MGS/SiO_2/TiO_2 tubes

$$[Pt(NH_3)_4][PtCl_4] \rightarrow 2Pt + 2N_2 + 4H_2 + 4HCl \quad (4)$$

According to the ratios in the molecular weight ($2Pt:[Pt(NH_3)_4][PtCl_4] = 390:598$ g/mol), the mass of the pure MGS should decrease by about 33%. The observed slightly higher mass loss (approx. 35%) can be explained with the inclusion of some water molecules in the salt. For the Pt/SiO_2 tubes, the weight loss is approximately 23%. A part of this loss (around 100 °C) is due to desorption of water presumably mainly for the silica walls. For the sharp decrease in mass observed at 270 °C resulting from the destruction of the MGS fibers, a mass loss of about 18% can be deduced. When compared to the 35% weight loss from pure MGS, this demonstrates that in tubes about 51 wt% of Pt particles was encapsulated.

The transmission electron micrographs shown in Fig. 8 further confirm the reduction of Pt salt to Pt metal at 280 °C. Figure 8a shows that abundant Pt was dispersed into the tubes upon reduction. Pt particles of diameter 5–10 nm are embedded in the SiO_2 matrix and distributed inside the whole tube wall. The sample was probed by dark-field imaging, which displays high amount of Pt incorporated inside the tubes (Fig. 8b). The tubes further portray thin silica walls (about 30 nm in thickness) with rectangular cross-section (compare Fig. 4b). Since the tubes possess rectangular cross-section, the density of the Pt metal was found higher along the walls than in the interior of the tubes. Pt particles were barely observed on the outer surface of SiO_2 tubes.

The selected area electron diffraction (SAED) pattern shown in Fig. 8c was obtained from a 1.2-μm circular region of a tube placed over a hole in the carbon support film. The crystallinity of the Pt particles as well as the amorphous state of SiO_2 could be well established from the

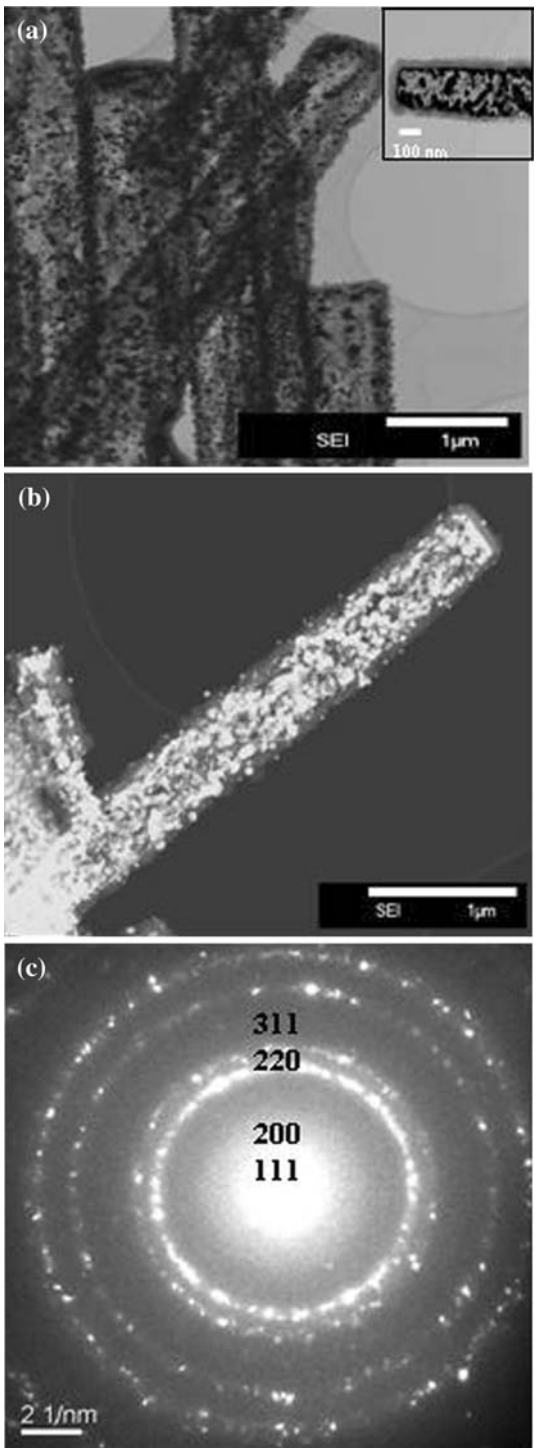

Fig. 8 **a** TEM micrograph demonstrating Pt-filled SiO_2 tubes. **b** Dark-field image of a single Pt/SiO_2 tube. **c** Selected area electron diffraction (SAED) pattern of Pt/SiO_2 tubes

pattern. It shows Debye–Scherrer rings that could be indexed according to face-cubic centered (fcc) platinum with a lattice constant of $a = 3.944$ Å which is close to the lattice constant for ideal Pt (fcc) crystals of 3.920 Å [52].

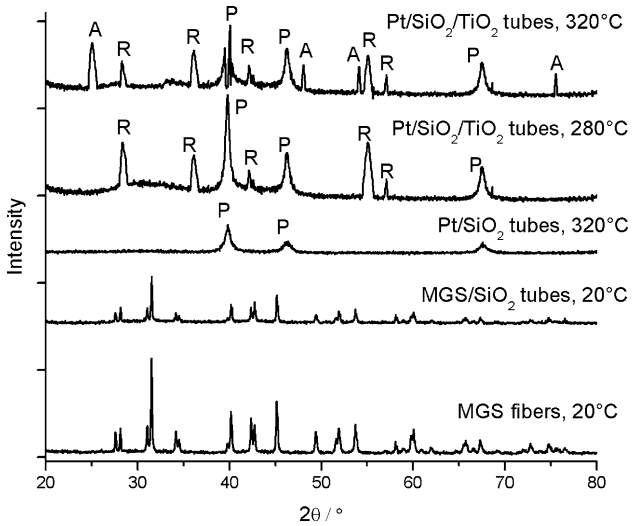

Fig. 9 XRD patterns of MGS fibers, MGS/SiO_2 tubes, and Pt/SiO_2 tubes calcined at 280 °C, Pt/SiO_2/TiO_2 tubes calcined at 280 °C, and Pt/SiO_2/TiO_2 tubes calcined at 320 °C. The peaks labeled *A*, *R*, and *P* are assigned to anatase, rutile, and Pt phase, respectively

Besides, the diffuse background can be attributed to the amorphous silica tube walls.

The powder XRD patterns of the templating MGS fibers, as-synthesized MGS/SiO_2 tubes, and calcined Pt/SiO_2 tubes are given in Fig. 9. The XRD pattern of the MGS template obtained by the reprecipitation with ethanol is almost similar to the XRD pattern of MGS/SiO_2 tubes; however, the intensity of the peaks in the latter is lower due to the presence of amorphous SiO_2. The peak positions are in good agreement with those calculated with lattice data given by Atoji et al. [43]. After calcination, the reflections of crystalline platinum (annotated as "P" in the Pt/SiO_2 pattern) fit also well with those given in literature [53]. Due to a distinct broadening of the peaks, the incorporated Pt particles can be regarded as being of nanometer size.

Pt nanoparticles in the SiO_2/TiO_2 tubes

Figure 10 represents the TEM images of Pt/SiO_2/TiO_2 tubes after calcination at 280 °C for 6 h in a stream of air. The TEM results are consistent with the SEM observations on the as-synthesized MGS/SiO_2/TiO_2 tubes. The tube ends are rectangular in morphology. The black spots in the tubes were identified as agglomerated Pt particles by EDXS analysis formed by the decomposition of MGS fibers during heat treatment. The thickness of the tube walls was found to depend on the contact time with the titanium containing solution before filtration. If the reaction time is only 2 min, the walls of the resulting NTs are very thin and irregular with a rather high Si/Ti ratio (Fig. 10a).

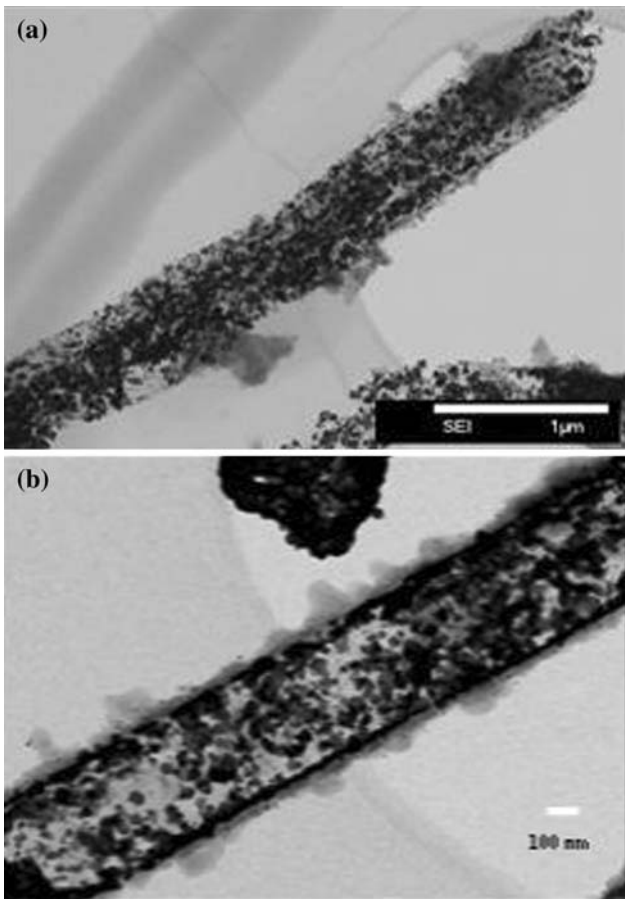

Fig. 10 TEM bright-field images of Pt/SiO_2/TiO_2 tubes with time of hydrolysis of 2 min (**a**) or 20 min (**b**)

Prolonging the reaction time to 20 min leads to more stable walls of about 30–40 nm thickness and high Ti content (Figs. 5d, 10b). The gray-colored parts on the walls represent clustered titania nanostructures. In contrast to SiO_2, which tends to form layered structures resulting in rather smooth walls of the tubes (Fig. 8a, b), titania grows predominantly three dimensionally leading to more particulate pore walls. Thus, walls consisting of titania must always be thicker to be continuous.

From the fact that the gases formed during the autoreduction process of the MGS (Eq. 4) evolve from the tubes, it is clear that their walls possess a distinct porosity. N_2 adsorption isotherms confirmed this for SiO_2 tubes made with $[Pt(NH_3)_4](HCO_3)_2$ as templating salt [54].

The thermal decomposition of the MGS fibers in SiO_2/TiO_2 tubes was quantitatively analyzed by thermogravimetry again (Fig. 6). For the Pt/SiO_2/TiO_2 tubes, the weight loss at around 270 °C is approximately 17%. When compared to the 35% weight loss from pure MGS, it can be concluded that 48 wt% of Pt particles were encapsulated

inside the tubes. This result is in good agreement with the EDXS results on individual tubes (44 ± 3 wt%).

Figure 9 depicts diffraction patterns of $Pt/SiO_2/TiO_2$ tubes calcined at temperatures of 280 and 320 °C. After calcination at 280 °C, all crystalline titania is present as rutile phase; the position of the observed reflections fitting well with the reference JCPDS File No**:** 4-0551. The presence of rutile phase is surprising since rutile is usually formed only at higher temperatures. In this case, however, on one hand, their nanosize, as indicated by a distinct line broadening, and, on the other hand, the close interactions with the MGS salt, forming Pt nanoparticles, and with the amorphous SiO_2 phase seem to stabilize the rutile phase. All typical Pt reflections are also present, their intensity, however, is higher than in Pt/SiO_2 tubes, indicating that the crystallization of the titania also enhances the crystallization of the Pt. Such phenomenon is often found in Pt/TiO_2 systems [55]. Calcination at a slightly higher temperature of 320 °C results in a mixture of rutile and anatase phase; the positions of the reflections of the latter agreeing well with the data in the reference (JCPDS File No: 21-1272). At this higher temperature, anatase, which is thermodynamically more stable in the temperature range up to about 600 °C, starts to form. Probably, during calcination, the autoreduction step (Eq. 4) precedes faster, impeding intimate interaction of the titania and the Pt phases. Thus, the rutile phase cannot be stabilized that well. Elevating the calcinations temperature further to 350 °C not only leads to more anatase phase but also deformation of the tubes into nanoparticles. This again confirms the trend that titania more likely grows three dimensionally than two dimensionally. The tubular structure seems to be better achievable with rutile particles being in close contact with amorphous silica and the platinum phases.

Conclusions

Pt-incorporated SiO_2 and SiO_2/TiO_2 tubes have been synthesized for the first time using fibrous MGS crystals as templating structures. Well-defined morphology, longer tubes, and higher Pt loadings (48–51 wt%) inside the tubes than found with other templating salts were obtained at low synthesis temperatures. This study demonstrates also that the fine tuning of the hydrolysis of TIP and its subsequent interaction with TEOS helped in achieving better coating of titanium alkoxide on the MGS crystal fibers. Moreover, the addition of TEOS not only impeded the aggregation of template fibers but also protected the deformation of the tubes from thermal and drying stresses. Structural and morphological characterizations showed that the tubes have smooth morphology with an average diameter of 500 nm and lengths in the broad range of 4–15 μm.

Acknowledgements The authors express their sincere gratitude to Dr. Falk Heinroth (Institute of Inorganic Chemistry, Leibniz University of Hannover) for performing TGA analysis and Prof. Dr. Jürgen Caro (Institute of Physical Chemistry, Leibniz University of Hannover) for general support. The work was financially supported by Deutsche Forschungsgemeinschaft (DFG, WA 1116-16).

References

1. Shi WS, Peng HY, Wang N, Li CP, Xu L, Lee CS (2001) J Am Chem Soc 123:11095
2. Li YC, Li XH, Yang CH, Li YF (2003) J Mater Chem 13:2641
3. Law M, Goldberger J, Yang PD (2004) Annu Rev Mater Res 34:83
4. Ohsaki Y, Masaki N, Kitamura T, Wada Y, Okamoto T, Sekino T, Niihara K, Yanagida S (2005) Phys Chem Chem Phys 7:4157
5. Mor GK, Shankar K, Paulose M, Varghese OK, Grimes CA (2006) Nano Lett 6:215
6. Martinson ABF, Elam JW, Hupp JT, Pellin MJ (2007) Nano Lett 7:2183
7. Varghese OK, Gong D, Paulose M, Ong KG, Grimes CA (2003) Sens Actuators B 93:338
8. Martin CR, Kohli P (2003) Nat Rev Drug Discov 2:29
9. Park J, Kim HS, Bard AJ (2006) Nano Lett 6:24
10. Fan R, Karnik R, Yue M, Li D, Majumdar A, Yang P (2005) Nano Lett 5:1633
11. Quan X, Yang S, Ruan X, Zhao H (2005) Environ Sci Technol 39:3770
12. Duan XF, Huang Y, Agarwal R, Lieber CM (2003) Nature 421:241
13. Kijima T, Yoshimura T, Uota M, Ikeda T, Fujikawa D, Mouri S, Uoyama S (2004) Angew Chem Int Ed 43:228
14. Goldberger J, He RR, Zhang YF, Lee S, Yan HQ, Choi HJ, Yang PD (2003) Nature 422:599
15. Hu JQ, Bando Y, Zhan JH, Goldberg D (2004) Angew Chem Int Ed 43:4606
16. Patzke GR, Krumeich F, Nesper R (2002) Angew Chem Int Ed 41:2446
17. Johnson BFG (2003) Top Catal 24:147
18. Qu J, Zhang X, Wang Y, Xie C (2005) Electrochim Acta 50:3576
19. Albu SP, Ghicov A, Macak JM, Schmuki P (2007) Nano Lett 7:1286
20. Shankar K, Mor GK, Prakasam HE, Yoriya S, Paulose M, Varghese OK, Grimes CA (2007) Nanotechnology 18:065707
21. Adachi M, Murata Y, Okada I, Yoshikawa S (2003) J Electrochem Soc 150:G488
22. Guisbiers G, Van Overschelde O, Wautelet M (2008) Appl Phys Lett 92:103121
23. Bavykin DV, Walsh FC (2009) Eur J Inorg Chem 8:977
24. Ghicov A, Schmucki P (2009) Chem Commun 2791
25. Nakahira A, Kato W, Tamai M, Isshiki T, Nishio K, Ariani H (2004) J Mater Sci 39:4239. doi:10.1023/B:JMSC.0000033405.73881.7c
26. Adachi M, Murata Y, Harada M, Yoshikawa S (2000) Chem Lett 29:942
27. Akita T, Okumura M, Tanaka K, Ohkuma K, Kohyama M, Koyanagi T, Date M, Tsubota S, Haruta M (2005) Surf Interface Anal 37:265
28. Arbiol J, Cirera A, Peiró F, Cornet A, Morante JR, Delgado JJ, Calvino JJ (2002) Appl Phys Lett 80:329
29. Epifani M, Helwig A, Arbiol J, Diaz R, Francioso L, Siciliano P, Mueller G, Morante JR (2008) Sens Actuator B 130:599
30. Sato Y, Koizumi M, Miyao T, Naito S (2006) Catal Today 111:164

31. Li Y, Ye CH, Fang XS, Yang L, Xiao YH, Zhang LD (2005) Nanotechnology 16:501
32. Lim YB, Bando YS, Goldberg D (2003) Adv Mater 15:581
33. Bae C, Yoo H, Kim S, Lee K, Kim J, Sung MM, Shin H (2008) Chem Mater 20:756
34. Mayya KS, Gittins DI, Dibaj AM, Caruso F (2001) Nano Lett 1:727
35. Sander MS, Côté MJ, Gu W, Kile BM, Tripp CP (2004) Adv Mater 16:2052
36. Caruso RA, Schattka JH, Greiner A (2001) Adv Mater 13:1577
37. Hippe C, Wark M, Lork E, Schulz-Ekloff G (1999) Micropor Mesopor Mater 31:235
38. Wark M, Hippe C, Schulz-Ekloff G (2000) Stud Surf Sci Catal 129:475
39. Ren L, Wark M (2005) Chem Mater 17:5928
40. Ren L, Guo M, Wark M, Hou Y (2005) Appl Phys Lett 87:212503
41. Ren L, He L, Chen C, Wark M, Li C, Che P, Guo L (2007) J Magn Magn Mater 312:405
42. Ohya T, Nakayama A, Ban T, Ohya Y, Takahashi Y (2002) Chem Mater 14:3082
43. Atoji M, Richardson JW, Rundle RE (1957) J Am Chem Soc 79:3017
44. Bremi J, Brovelli D, Caseri W, Hähner G, Smith P, Tervoort T (1999) Chem Mater 11:977
45. Interrante LV, Messmer RP (1971) Inorg Chem 10:1175
46. Sanchez C, Livage J, Henry M, Babonneau F (1998) J Non-Cryst Solids 100:65
47. Jiang X, Herricks T, Xia Y (2003) Adv Mater 15:1205
48. Sun YG, Xia YN (2004) Adv Mater 16:264
49. Delattre L, Babonneau F (1997) Chem Mater 9:2385
50. Pickup DM, Mountjoy G, Wallidge GW, Anderson R, Cole JM, Newport RJ, Smith ME (1999) J Mater Chem 19:1299
51. Rajesh Kumar S, Suresh C, Vasudevan AK, Suja NR, Mukundan P, Warrier KGK (1999) Mater Lett 38:161
52. Lümmen N, Kraska T (2005) Nanotechnology 16:2870
53. Qian HS, Antonietti M, Yu SH (2007) Adv Funct Mater 17:637
54. Ren L (2004) PhD thesis, University of Hannover, Germany
55. Ismail AA, Bahnemann DW, Bannat I, Wark M (2009) J Phys Chem C 113:7429